

CALCULATION OF THERMAL STRESSES IN GRAPHITE FUEL BLOCKS

Y. Lejeail*

*CEA Cadarache, DEN/DER/SESI/LCSI,
Bat. 212, 13108
Saint-Paul-Lez-Durance Cedex, France
Phone: 33 00 442257762, Fax: 7187
E-mail: yves.lejeail@cea.fr*

M.T. Cabrillat

*CEA Cadarache, DEN/DER/SESI/LCSI,
Bat. 212, 13108
Saint-Paul-Lez-Durance Cedex, France
Phone: 33 00 442257360, Fax: 7187
E-mail: mcabrillat@cea.fr*

ABSTRACT

This paper presents a parametric study of temperature and thermal stress calculations inside a HTGR core graphite block, taking into account the effect of fluence on the thermal and mechanical properties, up to $4 \cdot 10^{21}$ n/cm². The Finite Element model, realized with Cast3M CEA code, includes the effects of irradiation creep, which tends to produce secondary stress relaxation.

Then, the Weibull weakest link theory is recalled, evaluating the possible effects of volume, stress field distribution (loading factor), and multiaxiality for graphite-type materials, and giving the methodology to compare the stress to rupture for the structure to the one obtained from characterization, in the general case.

The maximum of the Weibull stress in Finite Element calculations is compared to the value for tensile specimens. It is found that the maximum of the stress corresponds to the end of the irradiation cycle, after reactor shutdown, since both thermal conductivity and Young's modulus increase with time. However, this behaviour is partly counterbalanced by the increase of material strength with irradiation.

Keywords: HTGR, Graphite Blocks, Thermal Stresses

1. INTRODUCTION

The High Temperature Gas cooled Reactors (HTGR) give the advantage of passive safety, in particular due to their high core equivalent thermal conductivity. Even if it is not imposed by design codes at this time, it should be better to calculate the thermal stress evolutions of graphite assemblies during their life, in order to avoid local cracking of these components, and thus to prevent any core damage or performance degradation.

As the graphite in the core is submitted to irradiation, thermal properties will change with fluence level and temperature of irradiation, leading to an evolution of the thermal loadings with time. Thus it is very important to know the influence of irradiation on graphite thermal properties; lot of works have been performed for the HTTR experimental reactor and have been published in the literature (see S. Ishiyama, T.D. Burchell, J.P. Strizak, M. Eto, (1996), as well as T. Oku, M. Ishihara, (2004)). So there is a large amount of consistent data available on the IG-110 graphite, allowing to adjust models, especially for the density and for the thermal conductivity. This material, although not chosen for the future European HTGR project, was a good choice to start our numerical study. Concerning the mechanical properties, the evolution of Young modulus as well as thermal expansion is also provided

by the above papers and by T. Oku, M. Eto, S. Ishiyama, (1990). Strength and irradiation creep properties changes must also be taken into account; the first one is known to increase with fluence, and the second one may relax the stresses during normal operating, causing residual stresses to appear at reactor shutdown.

During normal operating conditions, graphite blocks should be submitted to weight loads, temperature gradients induced by fuel power densities. Irradiation shrinkage of the graphite may modify the strains and the displacements in the assembly, but could also generate stresses if fluence gradients exist in the core, in the same way as the temperature act. Depending on the initial geometry and on the respective shrinkage of fuel elements and graphite blocks, some mechanical contacts may occur during irradiation cycle, creating additional stresses inside the blocks. All the transients should be included in a safety analysis (while it is not the subject of this paper), and it seems that cold thermal shocks are the most severe cases since graphite does not sustain tensile stresses as well as compressive ones (Iyoku T., Ueta S., Sumita J., Umeda M., Ishihara M., (2004)).

Last, the stresses which are calculated inside the components must be post-treated with a Weibull-like procedure. Since graphite material is brittle, the material strength depends on the volume which is really stressed. This can be divided in both a volume effect and a stress distribution factor (called "loading factor" in the literature). These two effects can be easily accounted for, by integration of the strain energy on the whole volume of the structure; however, a discussion and a validation of this kind of approach should be done, since it must be verified that material fabrication process, machining technique, and resulting flaw types inside the material are the same between characterization specimens and real components (or between several mechanical testing specimens). Chen and Ou (2004) discussed these points for the case of microelectromechanical systems. An other important feature is the difference of strength between tension and compression, which can be reproduced in the local stress criteria.

All these characteristics are detailed in the following paragraphs, which describe the principal options of the numerical model.

2. NUMERICAL MODEL DESCRIPTION

Cast3M CEA Finite Element code was used to carry out this study (Verpeaux P., Charras T. et Millard A., 1988). This code allows performing both thermal and mechanical analyses. The application has been done on a 600MWth HTGR with hexagonal graphite blocks; the core is annular and GT-MHR project was taken as reference (Kodochigov N., Sukharev Y., Marova E., Ponomarev Stepnoy N., Glushkov E., Fomishenko P., (2003)), although the model is intended to be applied for Very High Temperature parametric studies in the near future.

2.1 Mesh and Geometry

One twelfth of a graphite fuel block was modelized in Cast3M code (Fig. 1). Each assembly contains 216 fuel elements of 12.5 mm diameter and 108 coolant channels of 16 mm diameter. On the Figure 1, the holes are the coolant channels, while the red disks are the compact fuel elements. The minimum external width of the hexagonal assembly is 360 mm (across flats distance). The 2D mesh for the graphite assembly was build with 650 quadratic elements (6 nodes triangles or 8 nodes quadrangles).

A 37.5 mm diameter hole is placed at the center. It is intended to extend the capabilities of the mesh by representing a whole assembly (in view of representing dissymmetrical power loading) in further studies. In addition, it is planned to have a 3D version of the mesh to account for axial gradients of power profile.

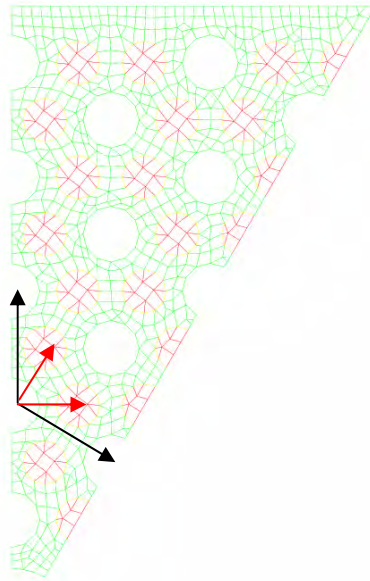


Fig. 1 View of the mesh of 1/12 of the hexagonal graphite fuel block. The arrows show how the mesh is generated, as the geometry can be seen as a network of coolant channels, with a pattern of two fuel elements for each coolant channel (in a crystallographic analogy)

2.2 Loading and boundary conditions

The fuel elements are included for the thermal calculation but are excluded for the mechanical part; it means that mechanical contact is not represented at the present time. This particular behaviour should be checked first by experimental tests. Figure 2 summarizes both the thermal and mechanical boundary conditions. Currently, the hypothesis for the mechanical part is the generalized plane strains condition which assumes that each cross section will remain a plane cross section.

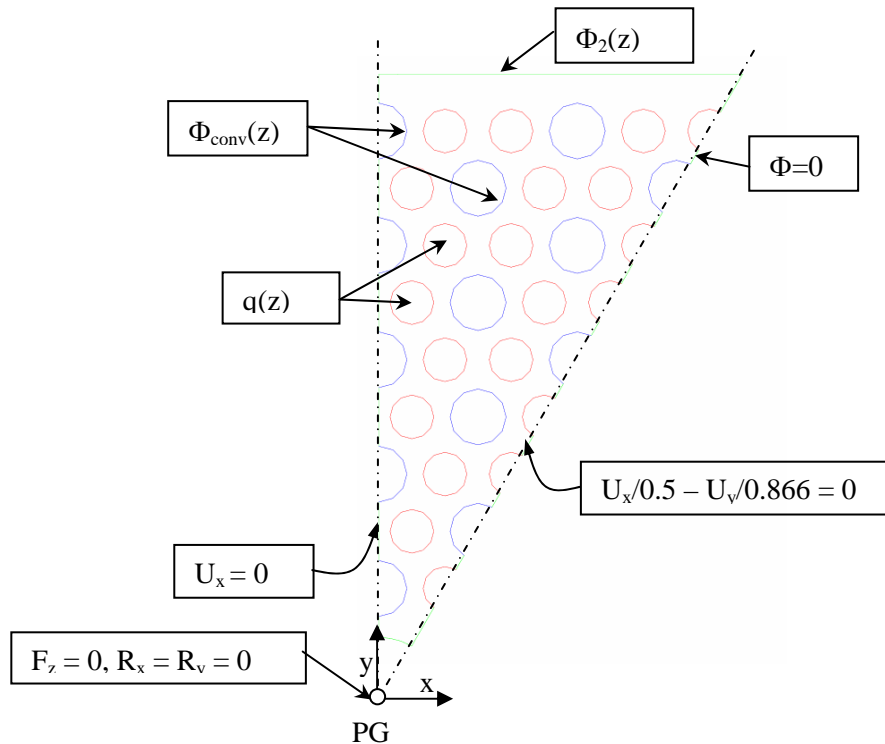


Fig. 2 Schema of thermal and mechanical loading, and boundary conditions

The end rotations of the generalized plane strains point (PG) are kept to zero, as well as the axial force at the same location, which means that the axial displacement of the whole section should follow the thermal expansion and irradiation shrinkage without stress, in case of uniform temperature loading.

2.2.1 Power densities

In each fuel element, is imposed a power density which is constant in a cross section but can vary along z axis with a cosine profile (Equation 1); in 2D, it means that we can calculate different block position along the axial core. In the model, $z = +L/2$ corresponds to the exit of the core while $z = -L/2$ refers to the inlet of the core.

$$q(z) = q_0 \cos\left(\frac{2\omega_a z}{L}\right) \quad (1)$$

The axial evolution must be related to the mean power density q_{mean} (Equation 2), the latter being itself linked to the specific power of the core G_0 (= total power P_{tot} divided by total core volume V_{tot}) using the fuel density d_{fuel} (=volume of fuel elements V_{fuel} divided by total core volume V_{tot}) as shown in Equation 3.

$$q_{mean} = q_0 \frac{\sin(\omega_a)}{\omega_a} = q_0 K_a \quad (2)$$

$$q_{mean} = \frac{P_{tot}}{V_{fuel}} = \frac{P_{tot}}{V_{tot} d_{fuel}} = \frac{G_0}{d_{fuel}} \quad (3)$$

2.2.2 Fluid temperatures and heat transfers

At the equilibrium state, the energy transfer must be written between the power inside a fuel column and the gas depending on the mass flow rate Q:

$$P(z) = d_{fuel} \int_{V_z} q dv = Q C_p (\theta(z) - \theta_e) \quad (4)$$

So that the fluid temperature can be determined using all equations (1) to (4):

$$\theta(z) = \theta_e + \frac{\theta_s - \theta_e}{2} \left[\frac{\sin\left(\frac{2\omega_a z}{L}\right)}{\sin(\omega_a)} + 1 \right] \quad (5)$$

The model is very basic and assumes that the power densities are constant in a horizontal core cross-section; this implies that the fluid temperatures will also be identical in a same core cross section. In order to take into account the radial power peak described by Kodochigov (2003), an additional peak coefficient $K_r = 1.5$ has been applied to all the above equations; thus, the results are representative of the hottest part of the core (corresponding to the internal radius). Using the parameters of Table 1, an exit helium temperature of 1030°C can be derived, which is in good agreement with the maximum 1000°C obtained by Kodochigov (2003).

Table 1 Main parameters for the calculation of power densities and fluid temperature profiles

| Total power | Mass flow rate | Specific power | Core Height | Power density axial coefficient | Fuel density | Axial peak factor | Inlet fluid temperature | Maximum fluid temperature |
|-------------------|----------------|-------------------------------|-------------|---------------------------------|--------------|-------------------|-------------------------|---------------------------|
| P_{tot} (MW) | Q (kg/s) | G_0 (W/mm ³) | L (m) | ω_a | d_{fuel} | K_a | θ_e (°C) | θ_s (°C) |
| 600 | 320 | $6.55 \cdot 10^{-3}$ | 8 | $0.83 \pi / 2$ | 0.265 | 1/1.352 | 480 | 1030 |

Finally, the famous Dittus-Boelter (1930) correlation has been used for the forced convection helium heat transfer coefficient; it led to a mean coefficient $h = 2500 \text{ W/m}^2/\text{°C}$ utilized by Cast3M in the calculation of Φ_{conv} thermal flux in the coolant channels (see Fig. 2):

$$\Phi_{conv} = h (T_s - \theta) \quad (6)$$

The code simply evaluates the surface temperature (T_s) of the blocks inside coolant channels knowing the fluid temperature θ given by Equation (5).

At the external side of the hexagon, an other heat transfer coefficient (h_2) has been imposed, as there is a by-pass fluid flow between blocks; this coefficient has been arbitrarily set to $10 \text{ W/m}^2/\text{°C}$ to evaluate the Φ_2 heat flux on Figure 2. A parametric study could be done to estimate the influence of this parameter which may be important, knowing that the total mass flow rate is equal to the sum of by-pass mass flow rate and the core mass flow rate. A higher heat transfer coefficient at the external side of the assemblies means a lower heat transfer inside the coolant channels due to the Dittus-Boelter relation.

2.2.3 Evolution with time

The fuel cycle is assumed to be 841 days long. The evolution of power and temperature are imposed as follows:

- at the initial state, the blocks are supposed to have a homogeneous temperature of 480°C equal to fluid temperature, with no power;
- the full power is reached in one day, as well as the permanent state fluid temperatures defined by Equation (5);
- end of irradiation is set at 840 days;
- the residual state for which the fluid temperature will come back to 480°C and the core will have no power, is defined at the time 841 days.

Three states are interesting to look at: the beginning of the irradiation, the end of irradiation, and the residual state.

2.3 Graphite properties

A simple thermal conductivity law has been defined to reproduce the decrease of thermal conductivity with both temperature and fluence ϕ :

$$\lambda(T, \phi) = \lambda_0 [1 + \beta(T) \exp(-\gamma\phi)] \quad (7)$$

In this formulation, $\beta(T)$ is a polynomial function of the second degree. This model predicts a saturation effect for high doses, consistently with experiments of Ishiyama S., Burchell T.D., Strizak J.P., Eto M., (1996). But it seems to fail to reproduce the difference of thermal conductivity decrease with irradiation temperatures (the highest is the irradiation temperature, the lowest is the thermal

conductivity decrease with irradiation dose, according to Oku T., Ishihara M., (2004)). This phenomenon looks like a recovery process induced by temperature, and reduces the irradiation effect. The coefficients of identification are shown on Table 2 whereas the thermal conductivity for different temperature and fluence levels is illustrated on Figure 3.

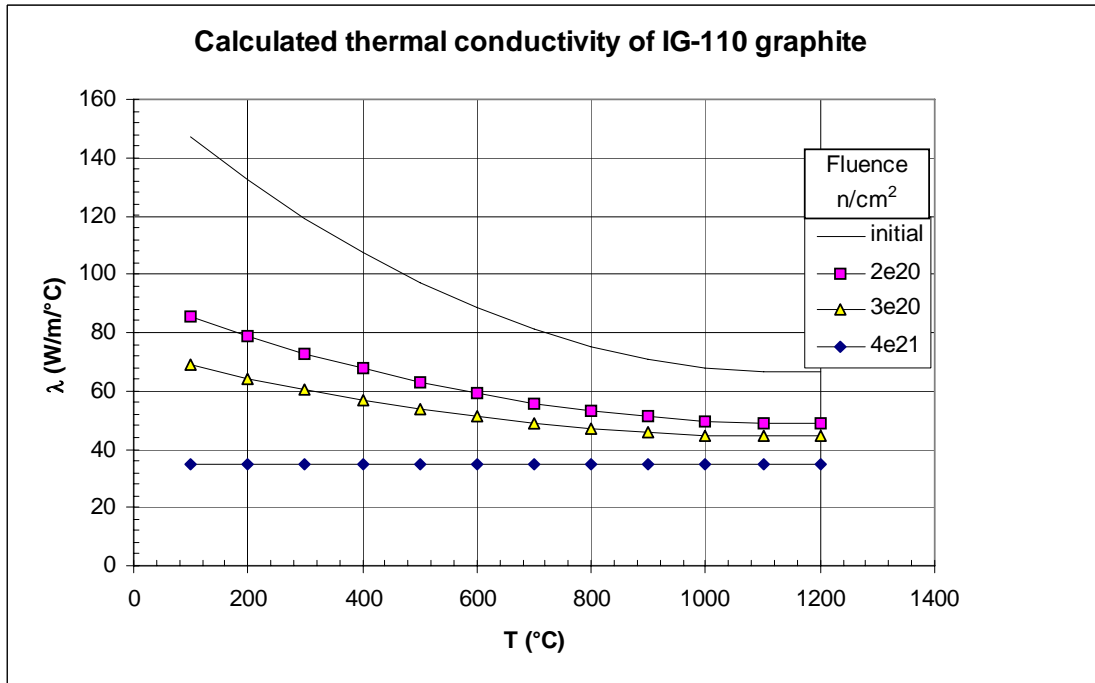


Fig. 3 Thermal conductivity versus temperature and fluence calculated for IG-110

The irradiation behaviour of the graphite has also been extensively studied by the same authors. They have confirmed a classical result for other graphite materials, i.e. the volume change is strongly temperature dependent. The IG-110 is a fine grain isotropic material, so that the dimensional changes were found approximately identical in all the directions. Densities, volume changes, and linear dimensional changes are thus closely and simply related by Equation 8:

$$\frac{\rho(t) - \rho_0}{\rho_0} = \frac{\Delta\rho}{\rho_0} = -\frac{\Delta V}{V_0} = -3\frac{\Delta L}{L_0} = -3f(\phi) \quad (8)$$

$$f(\phi) = f_0 + f_1\phi + f_2\phi^2 \quad (9)$$

The irradiation function $f(\phi)$ is a parabolic function of fluence as described in Equation 9, and it was found that parameters of Table 2 and Equation 9 give a good approximation of Ishiyama S., Burchell T.D., Strizak J.P., Eto M., (1996) and Oku T., Ishihara M., (2004) experimental data, although they can not reproduce the influence of the temperature.

Table 2 Coefficients for Equations (7) (8) (9). $\Delta L/L_0$ must be in %, ϕ in n/cm^2 , and T in °C in these formulas

| f_0 | f_1 | f_2 | β_0 | β_1 | β_2 | λ_0 (W/m°C) | γ |
|----------------------|---------------------------|--------------------------|-----------|----------------------|----------------------|---------------------|--------------------|
| $4,42 \cdot 10^{-2}$ | $-2,61546 \cdot 10^{-22}$ | $7,31102 \cdot 10^{-45}$ | 3,66257 | $4,83 \cdot 10^{-3}$ | $2,10 \cdot 10^{-6}$ | 35 | $4 \cdot 10^{-21}$ |

The calculated dimensional changes due to irradiation are plotted on Figure 4. Note that this change is set in Cast3M code to influence both the thermal properties (by mean of density) and the irradiation dimensional change (in the 2D model, an additional thermal strain is imposed depending on the level of local fluence, also following Equation 1).

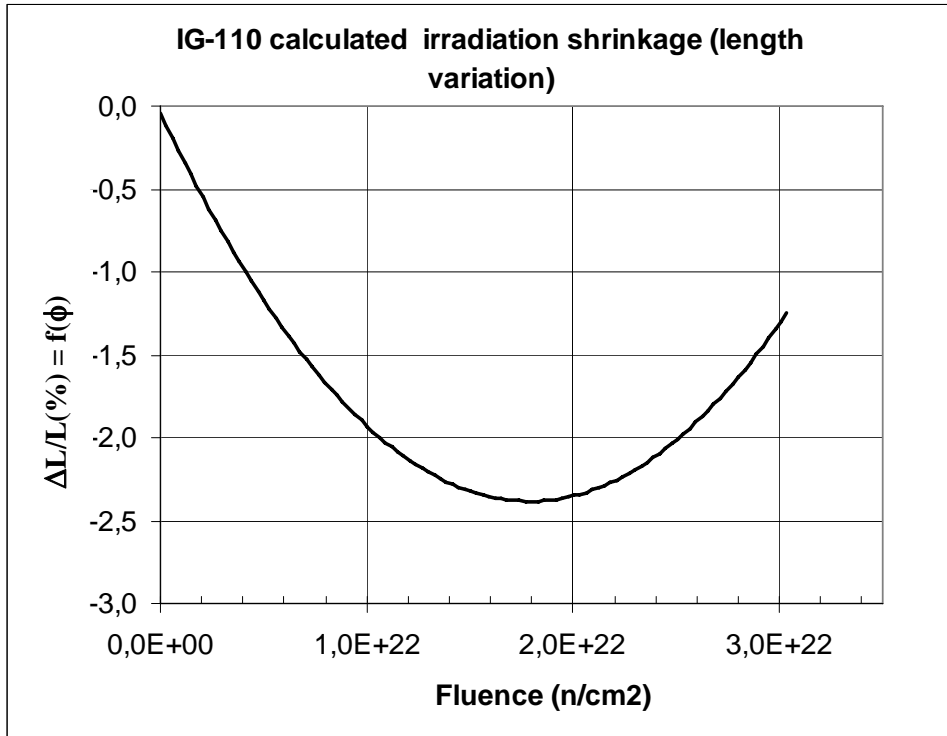


Fig. 4 Calculated mean dimensional variation for IG-110

The same function was applied to describe the Young's modulus changes after irradiation, according to the same authors results. An unusual power law function was necessary to fit the experimental data as can be seen in Table 3 and Equation 10:

$$\frac{E(t)}{E_0} = \left[1 + n \left(\frac{\rho(t) - \rho_0}{\rho_0} \right) \right]^m = [1 - 3nf(\phi)]^m \quad (10)$$

Table 3 : coefficients for the evolution of Young's modulus and irradiation creep, if $f(\phi)$ is in %.

| n | m | E_0 (MPa) | K (MPa/cm ²) ⁻¹ |
|---|-----|-------------|--|
| 2 | 0,3 | 10200 | $3.2 \cdot 10^{-25}$ |

To describe the effect of open porosity, the m exponent is usually known to be between 1 and 4 for ceramics (see Wagh A.S., Poeppel R.B., Singh J.P., (1991)). The discrepancy with this common evolution law is explained by Hall G., Marsden B.J., Fok S.L., Smart J., (2003) by the term of pinned dislocations appearing very rapidly during irradiation, compared to the open porosity variation term that may follow the dimensional evolution. Equation 10 and coefficients of Table 3, which try to combine these two effects, lead to an unusual m exponent. The relative evolution of Young's modulus after irradiation is given on Figure 5; the turnaround of the curve is correctly representing the experimental data of Ishiyama S., Burchell T.D., Strizak J.P., Eto M., (1996).

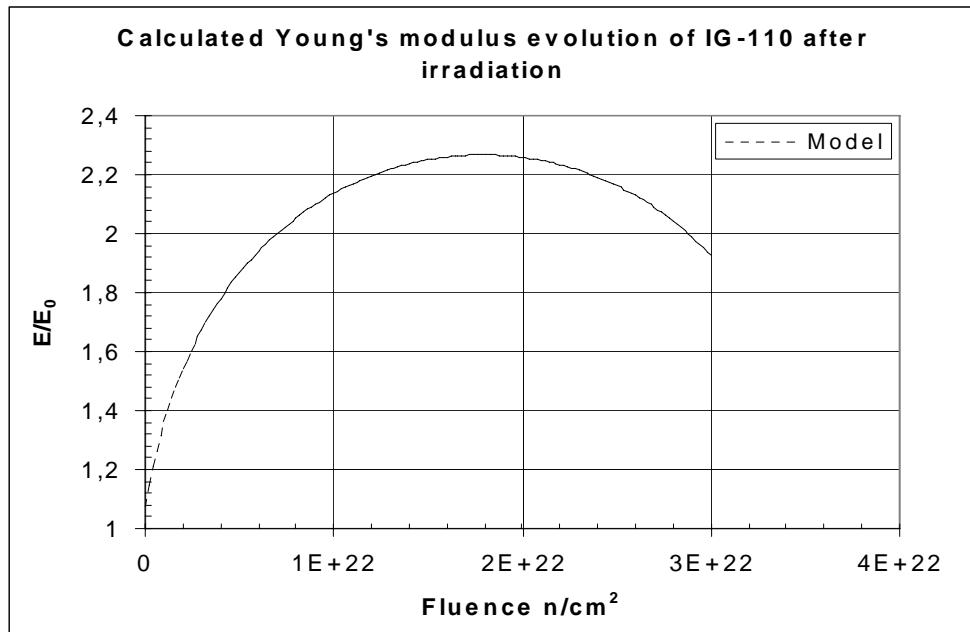


Fig. 5 Calculated Young's modulus for IG-110 under irradiation

The irradiation creep strain ε_c is given by a classical linear law in respect of the applied stress σ and the fluence ϕ :

$$\varepsilon_c (T, \phi) = K \sigma \phi \quad (11)$$

With Oku T., Eto M., Ishiyama S., (1990) experimental data, we have derived a minimum value of K given in Table 3. To complete the description, it should be said that Poisson's coefficient is taken equal to 0.15.

Thermal conductivity and density of fuel element are respectively taken to 10 W/m/°C and 1770 kg/m³ and are considered as constants due to the lack of data on this heterogeneous material. These values should not influence the calculation of the temperatures inside the graphite as the heat flux coming from the fuel element is just defined by the ratio of the power divided by the outer surface of the fuel compact.

2.4 Description of the different cases

Four calculations are interesting to describe here. The differences between the simulations are essentially the insertion of poisons in some places: no power is imposed in a poison compact, but the total power in an assembly is kept at the same level, so that the power densities are increased in the real fuel elements as shown on Table 4.

Table 4 Options of the different Finite Element calculations

| N° calculation | poison at coins block total of 6 per block | poisons at faces block total of 12 per block | max power density W/mm ³ | position of assembly in the core |
|----------------|---|---|--|-------------------------------------|
| 1 | no | no | 0,0335*216/216*1,5 | near outlet |
| 2 | yes | no | 0,0335*216/210*1,5 | near outlet |
| 3 | yes | yes | 0,0335*216/198*1,5 | near outlet |
| 4 | yes | no | 0,0335*216/210*1,5 | middle |

Basically, cases 1 to 3 are about an assembly placed at the maximum temperature level in the core, just before the outlet ($z = +2L/5$). Case 4 corresponds to an assembly at the maximum power density (i.e. $z = 0$). In calculation 1, there is no poison compact. In case number 2, there are 6 poison elements

at the angles of the hexagonal assembly, leading to only one/half of poison in the model representing one twelfth of an assembly. In case number 3, 12 other poison compacts have been added in the assembly, equivalent to one element for one twelfth of assembly. The exact position of this additional poison element is reported on Figure 6.

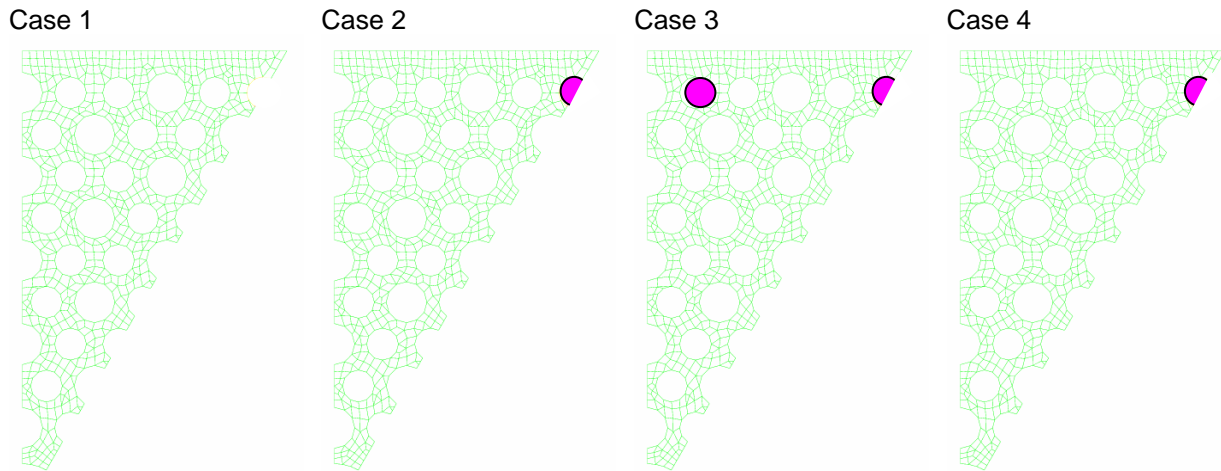


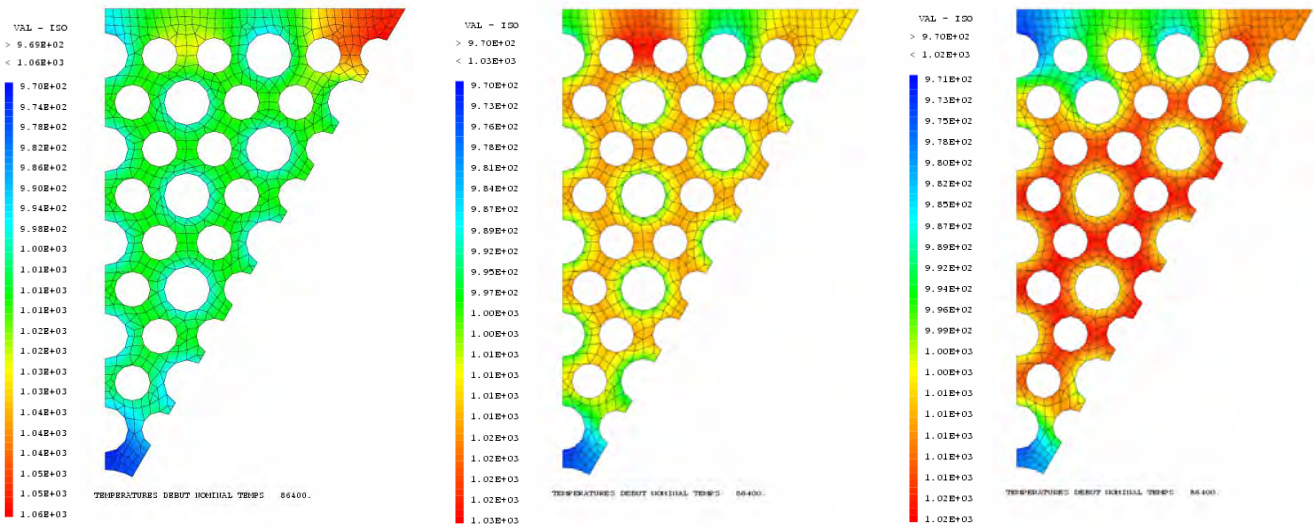
Fig. 6 Schema of poison element position in the calculations

The effect of the placement of a poison element can clearly be seen on the results of temperature and stresses.

4. NUMERICAL RESULTS

4.1 Temperatures

Temperature results at the beginning of irradiation are shown on Figure 7. The poison at the hexagonal angle causes a local decrease of the maximum temperature ($\sim 30^{\circ}\text{C}$, Case 2 compared to 1). As a result, the temperatures are more homogeneous in the assembly. An additional poison will only decrease further the temperature by 10°C (Case 3 compared to 2). The coldest point is always at the center of the graphite assembly: this can be attributed to the influence of the nearest coolant channel and could be optimized by decreasing the diameter of this channel, allowing to increase the distance between this channel and the central hole.

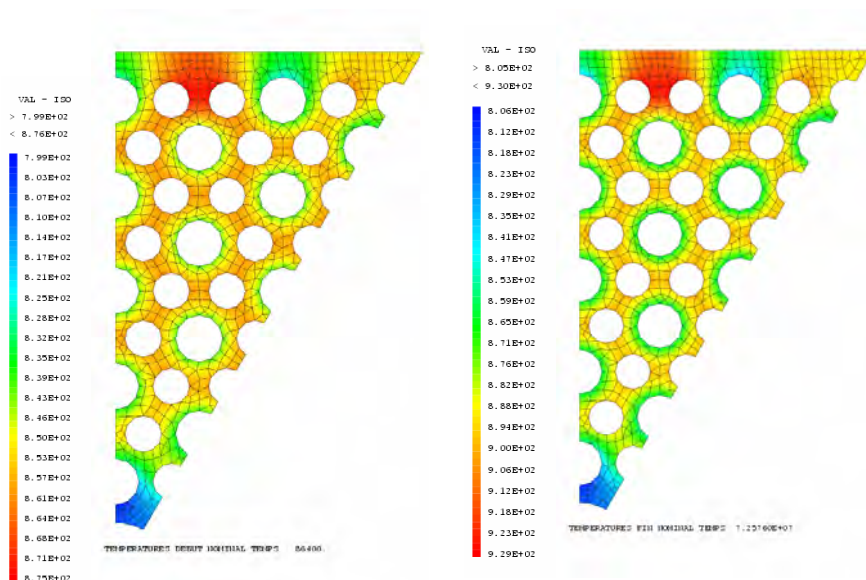


Case 1 : $T_{\max} = 1060^{\circ}\text{C}$ Case 2 : $T_{\max} = 1030^{\circ}\text{C}$ Case 3 : $T_{\max} = 1020^{\circ}\text{C}$

Fig. 7 Temperatures of graphite blocks at the beginning of irradiation (one day after start-up)

Case 4 represented on the Figure 8 gives the same temperature pattern as Case 2 but with a maximum temperature that is 155°C lower, since the assembly is at the middle of the core; the gradients are much higher than at the exit of the core (the power densities being higher).

At the end of irradiation, it was found an increase of temperature around 50°C for all cases due to the decrease of thermal conductivity as can be seen on the values of Figure 8. So a competition process between irradiation creep (relaxing the stresses) and both thermal conductivity decrease and Young's modulus increase (causing the stresses to increase) could be foreseen.



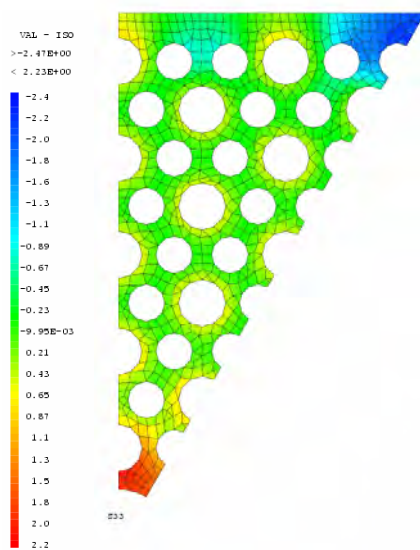
Case 4 : $T_{\max} = 875^{\circ}\text{C}$, $t = 1$ day Case 4 : $T_{\max} = 929^{\circ}\text{C}$, $t = 840$ days

Fig. 8 Evolution of the temperatures of graphite blocks for calculation number 4

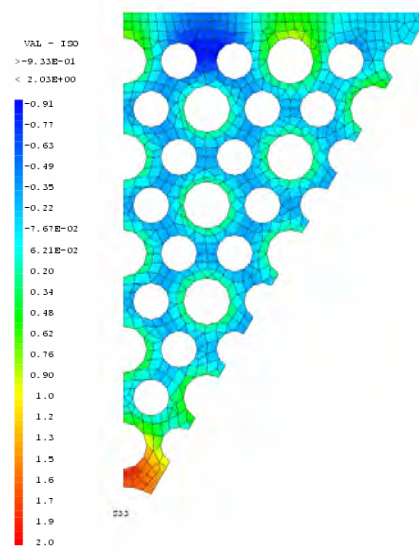
4.2 Stresses

Stress evolution can be summarized as follows:

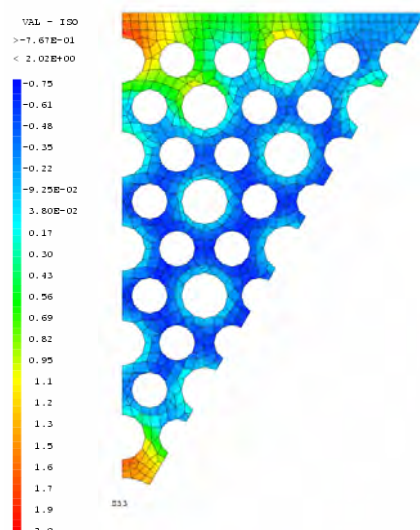
- at the beginning of irradiation (Figure 9), axial stresses are tensile in the coldest parts (near the central hole), and compressive near the highest temperature regions. The former are more damaging for graphite compared to the latter;
- then the irradiation creep relaxes the stresses which tend to zero at the end of irradiation, at full power. Increase of stress due to thermal conductivity and Young's modulus changes are not sufficient to counterbalance this effect, in the present study;



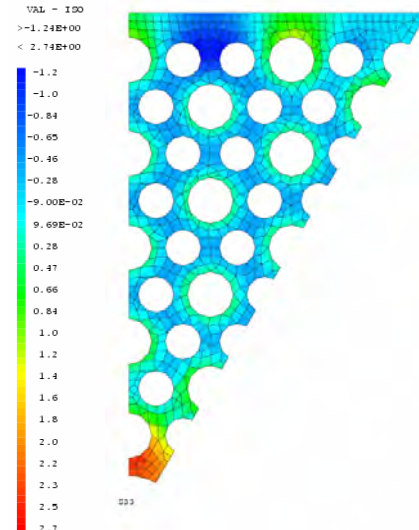
Case 1 :



Case 2 :



Case 3 :



Case 4 :

Fig. 9 Axial stresses at the beginning of irradiation (time equal to 1 day)

- thus, after reactor shutdown (Figure 10), the zones initially in tension become compressed, and the zones initially in compression become in tension. The values are much higher than the initial ones because of the effect of irradiation on thermal and mechanical properties.

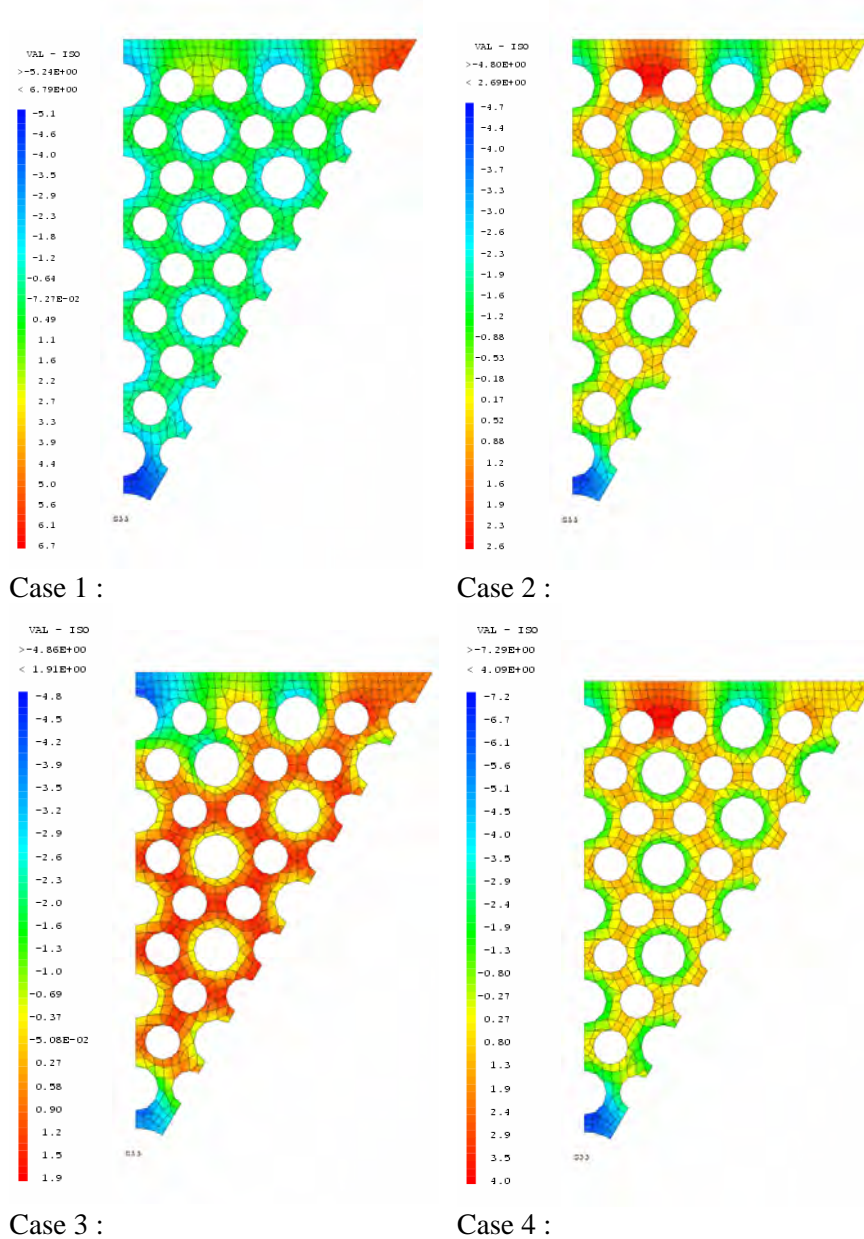


Fig. 10 Residual axial stresses after final cooling (time equal to 841 days)

A case-by-case comparison is also interesting since we can conclude to a very high gain in residual stress level when a poison is added at the assembly corners (Case 2 compared to 1, Figure 10). This amelioration is of course only seen at the end and does not exist at the beginning of irradiation, when the hottest points are in compression. Adding an additional poison element seems to improve the stress levels (Case 3 compared to number 2). The stresses are always higher at the middle of the core where the power densities are higher in our model (Case 4 compared to 2).

4.3 Weibull post-treatment

As the graphite material is brittle, it is necessary to apply a probabilistic theory to interpret the stress results. For a non-singular stress field, the Weibull weakest link theory can be applied on the assembly (Weibull, 1939). This theory simply considers the structure as a chain, so that the survival of the whole chain is equal to the survival of all links.

If the structure has a volume V_1 , the survival probability from Weibull weakest link model, can be written as follows for a two parameter law:

$$P_{sV_1} = \exp\left(-\frac{1}{V_0} \int_{V_1} \left\langle \frac{\sigma}{\sigma_0} \right\rangle^m dV\right) \quad (12)$$

V_0 is a reference volume, σ_0 is a reference stress corresponding to a rupture probability of 0.632 for the reference specimens (i.e. characterization tests). The Weibull modulus m can be seen as an indicator of material quality, since $m = 0$ corresponds to a poor reliability (fracture may appear for any stress with the same probability) and $m = \infty$ corresponds to a perfect material (fracture stress σ_0 is independent on volume and stress distribution). The brackets mean that only the positive terms are taken into account: this point should be modified for graphite since the material can also fail in compression (see below).

Equation 12 may be rewritten to point out two important effects, introducing the maximum stress in the structure σ_{\max} :

$$P_{sv1} = \exp\left(-\frac{V_1}{V_0} \left(\frac{\sigma_{\max}}{\sigma_0}\right)^m \frac{1}{V_1} \int_{V_1} \left\langle \frac{\sigma}{\sigma_{\max}} \right\rangle^m dV\right) \quad (13)$$

Then, it is interesting to look at the stress giving the same survival probability for a characterization specimen compared to a complex structure: that is the meaning of Equation 14.

$$\frac{\sigma_{rV_0}}{\sigma_0} = \left(\frac{V_1}{V_0}\right)^{\frac{1}{m}} \frac{\sigma_{\max}}{\sigma_0} L_{\max}^{\frac{1}{m}} \quad \text{with} \quad L_{\max} = \frac{1}{V_1} \int_{V_1} \left\langle \frac{\sigma}{\sigma_{\max}} \right\rangle^m dV \quad (14)$$

The stress in the characterization specimen σ_{rV_0} is related to the maximum stress in the component σ_{\max} , by mean of a volume effect $(V_1/V_0)^{1/m}$, and by a stress distribution factor $L_{\max}^{1/m}$. The larger is the volume V_1 , the lower will be the maximum stress σ_{\max} . The distribution factor L_{\max} explains why the stresses are larger in bending tests, compared to stresses in pure tensile specimens. Thus, there is no need to verify a membrane limit, bending limit, or peak stress limit with this approach, because the influence of stress profile is included in the L_{\max} integral. This equation must be carefully applied: in fact, it must be validated by experiments. The key point is that the type of defects which influence the rupture in the laboratory specimens must be the same than those which are present in the nuclear component. It is not so simple because it would depend on the stress profile, fabrication process, machining...

In Finite Element calculations, an equivalent stress S_{eq} for the structure may be defined without explicitly calculating the L_{\max} factor that is convenient for analytical analyses, and directly compared to the stress allowable on characterization specimen σ_{rV_0} :

$$S_{eq}^m = \frac{1}{V_0} \int_{V_1} \sigma_{eq}^m dV = \sigma_{rV_0}^m \quad (15)$$

The σ_{eq} local stress may include some triaxiality effects by mean, for instance, of the Maximum Strain Energy criteria (Rathjen, 1989), using the principal stresses Σ_i :

$$\sigma_{eq}^m = \sqrt{\Sigma_1^2 + \Sigma_2^2 + \Sigma_3^2 - 2\nu(\Sigma_1 \Sigma_2 + \Sigma_2 \Sigma_3 + \Sigma_1 \Sigma_3)}^m \quad (16)$$

This equation permits to include the effect of compressive stresses, replacing Σ_i by $\Sigma_i \sigma_t/\sigma_c$ if $\Sigma_i < 0$, σ_t and σ_c being respectively the graphite strength in tension and in compression

Note that the equivalent stress on the whole component may be expressed as a function of the already defined σ_{max} , V_1/V_0 , and L_{max} variables by means of Equation 17, simply combining (14) and (15).

$$S_{eq} = \left(\frac{V_1}{V_0}\right)^{\frac{1}{m}} \sigma_{max} L_{max}^{\frac{1}{m}} \quad (17)$$

We have applied Equation 15 on the graphite blocks using $V_0 = 10 \times 10 \times 100 \text{ mm}^3$ as a reference volume, and $m = 15$ for graphite Weibull's modulus.

The results reported on Figure 11 show the evolution of the equivalent stress during all the component life. The first part corresponds to an increase up to the full power time (1 day), then the stress decrease during all the irradiation cycle. The last part, appearing vertical on the figure, deals with the shutdown of the reactor (residual stress state).

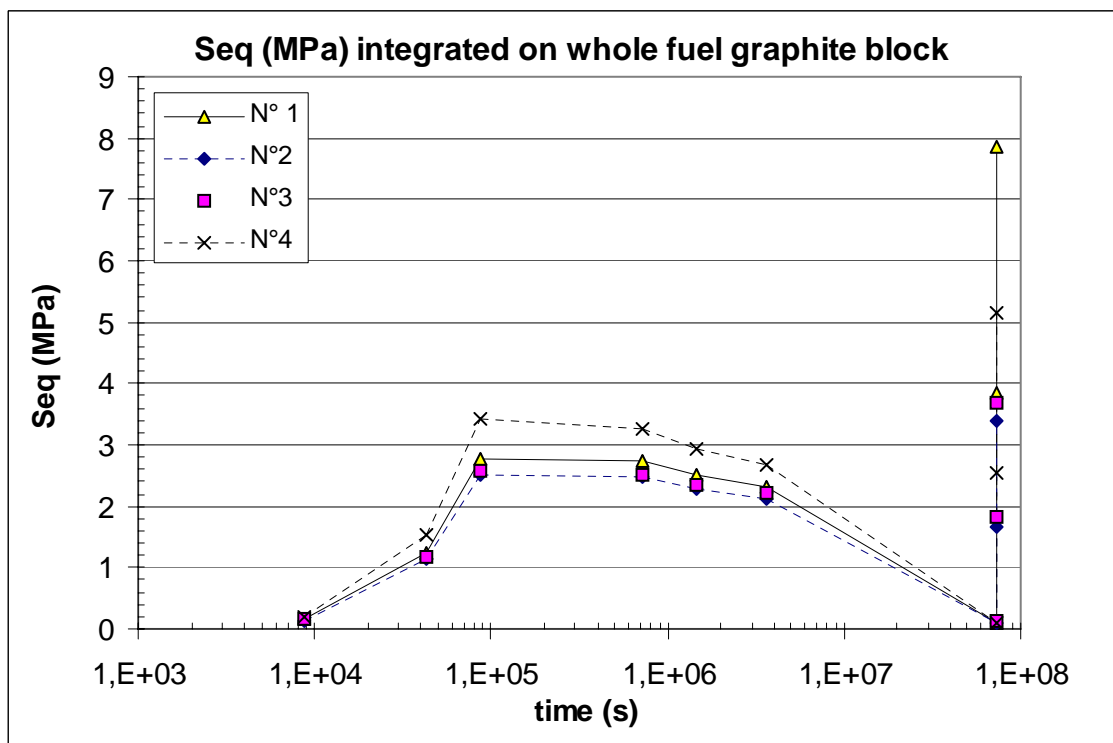


Fig. 11 Weibull equivalent stress on the whole structure taking Maximum Strain Energy criteria, equal to the stress giving the same rupture probability on characterization specimens curves

The maximum stress is confirmed to be at the end of life in our study, due to irradiation effect on thermal and mechanical properties. Case 1 without poison compact is the worst possible configuration. It is also confirmed that stresses will be higher at the level of the maximum power density. Comparison between Case 2 and 3 shows that improvements could be done in the placement of compacts inside the assembly.

Whether the calculated stresses are acceptable or not is not easy to estimate, but roughly speaking, the allowable stress should be equal to $\sigma_{tV0}(\phi=4 \cdot 10^{21} \text{ n/cm}^2) = 1.6 \sigma_0(\phi=0)/3$. Coefficient 1.6 is to take into account the increase of strength with irradiation, and in this example a margin of 3 is applied to the mean σ_0 stress. This coefficient should be defined in relation to material reliability, i.e. m Weibull's modulus, to reach a given rupture probability depending on the loading level. Let us assume a $\sigma_0 = 18$ MPa as a classical value, it means that the allowable design tensile stress could be as high as $\sigma_{tV0}(\phi=4 \cdot 10^{21} \text{ n/cm}^2) = 9.6$ MPa, corresponding to a rupture probability of $8 \cdot 10^{-5}$ for the initial material and $7 \cdot 10^{-8}$ for the irradiated graphite. The calculated stresses are all below this allowable stress, but it is sure that a middle core assembly with Case 1 configuration will exceed this stress limit.

5. CONCLUSIONS

A simplified model has been used in Cast3M Finite Element code to calculate the temperatures and stresses in fuel graphite blocks of a HTGR, focusing on the evolution of the results with irradiation. IG-110 graphite material has been chosen due to the material properties available in the literature. The influence of the position of poison fuel elements in the block has been pointed out, both on maximal temperatures and stresses:

- at full power, and at the beginning of irradiation cycle, the maximum tensile stresses in the blocks are in the cold temperature regions;
- the stresses are completely relaxed at the end of the irradiation cycle;
- thus, the residual stresses at reactor shutdown are in tension in the regions that were previously the hottest parts of the assembly.

Irradiation decreases the thermal conductivity and increases Young's modulus so that the residual stresses are higher than initial stresses. Taking into account the effect of the irradiation on strength, it has been found that Weibull equivalent stress on the whole structure would be under the allowable maximum tensile stress, except in the worst case (without poison element, and at the middle of the core). This study also demonstrated that it is possible to improve the configuration of fuel elements inside the assembly, in order to decrease maximum temperatures, temperature gradients, and stresses. However, neutronic studies should be performed to validate the simplified power density assumption.

REFERENCES

- [1] Ishiyama S., Burchell T.D., Strizak J.P., Eto M., (1996), Journal of Nuclear Materials, Vol. 230, pp. 1-7
- [2] Oku T., Eto M., Ishiyama S., (1990), Journal of Nuclear Materials, Vol. 172, pp 77-84
- [3] Oku T., Ishihara M., (2004), Nuclear Engineering and Design, Vol. 227, pp. 209-217
- [4] Iyoku T., Ueta S., Sumita J., Umeda M., Ishihara M., (2004), Nuclear Engineering and Design, Vol. 233, pp. 71-79
- [5] Chen K.-S., Ou K.-S., (2003), Sensors and Actuators A, Vol.112, pp. 163-174
- [6] Verpeaux P., Charras T. et Millard A., 1988, CASTEM 2000 une approche moderne du calcul des structures, in « Calcul des structures et intelligence artificielle », Fouet J.M., Ladevèze P., Ohayon R., Eds, Pluralis, 1988, p. 261-271
- [7] Kodochigov N., Sukharev Y., Marova E., Ponomarev-Stepnoy N., Glushkov E., Fomishenko P., (2003), Nuclear Engineering and Design, Vol. 223, pp 161-171
- [8] Dittus F. W., Boelter L. M. K. (1930), University of California Publications on Engineering, Vol. 2, p. 43, Berkeley, California.
- [9] Wagh A.S., Poeppel R.B., Singh J.P., (1991), Journal of Nuclear Materials, Vol. 26, pp. 3862-3868
- [10] Hall G., Marsden B.J., Fok S.L., Smart J., (2003), Nuclear Engineering and Design, Vol. 222, pp. 319-330
- [11] Weibull W., (1939), Proceedings of the Royal Swedish Institute, Engineering research, n° 151, Stockholm, Sweden
- [12] P. Rathjen, (1989), « Analysis of the Graphite Side Reflector Block of the HTR-Module », Proceedings of the Workshop on "Structural Design Criteria for HTR", Jülich, 31 January – 1 February 1989